

Refinement of A356 alloy using continuous rheological extrusion Al-Ti-V-B master alloy

Hong-fei Jia^{1,2}, *Guang-zong Zhang^{1,2}, Shuo Zhang^{1,2}, Da Teng^{1,2}, Qing He^{1,2}, Jun-wen Li^{1,2}, and Ren-guo Guan^{1,2}

1. Engineering Research Center of Continuous Extrusion, Ministry of Education, Dalian Jiaotong University, Dalian 116028, Liaoning, China

2. Key Laboratory of Near-Net Forming of Light Metals of Liaoning Province, Dalian Jiaotong University, Dalian 116028, Liaoning, China

Copyright © 2025 Foundry Journal Agency

Abstract: Based on thermodynamic calculations and continuous rheological extrusion (CRE) technology, Al-Ti-V-B master alloys were designed and prepared. The morphology and the distribution of the refined phases in the master alloys were analyzed by XRD, SEM, and TEM. The effects of master alloy addition and holding time on the microstructure and mechanical properties of A356 alloy were investigated. Under the optimum refiner addition of 0.3wt.% and the holding time of 20 min, the average grain size of the refined A356 alloy is $151.8 \pm 9.11 \mu\text{m}$, 89.62% lower than that of original A356 alloy. The tensile strength and elongation of as-cast A356 refined alloy are 196.11 MPa and 5.75%, respectively. After T6 treatment, the tensile strength and elongation of A356 refined alloy are 290.1 MPa and 3.09%, respectively. The fracture morphology is characterized by a predominance of along-crystal fracture with a small amount of through-crystal fracture, attributed to the refined grains. Finer grains promote crack path deflection and localized plastic deformation, enhancing energy dissipation and reducing the tendency for brittle fracture. This study provides a novel approach to improving the mechanical properties of A356 alloy through grain refinement using CRE Al-Ti-V-B master alloy.

Keywords: A356 alloy; continuous rheological extrusion; grain refinement; Al-Ti-V-B master alloy; mechanical properties

CLC numbers: TG146.21

Document code: A

Article ID: 1672-6421(2025)02-222-09

1 Introduction

A356 alloy is a hypoeutectic Al-Si alloy with low density, superior castability, and high strength, which is widely used in aerospace, transportation and other fields. The rapid development of industry puts forwards the higher demands on the properties of A356 alloy. However, the coarse α -Al dendrites of the alloy adversely affect its mechanical properties^[1,2]. Grain refinement is indispensable for the manufacture of aluminum alloy^[3-5]. Common methods of aluminum alloy refinement include adding grain refiner^[6-8], applying ultrasonic field^[9] or electromagnetic field^[10], increasing subcooling^[11], and pressure machining^[12,13]. Among them, adding grain refiner is the most cost-effective method. The grain size

is refined due to high nucleation rate and inhibition of grain growth^[14]. Various theories, including the carbide-boride theory^[15,16], component supercooling theory^[17], peritectic theory^[18], dual nucleation theory^[19], and solute theory^[20,21], are usually adopted to describe the mechanism of grain refinement.

Common grain refiners are Al-Ti-B and Al-Ti-C based master alloys, in which TiB_2 and TiC particles are used as substrate for heterogeneous nucleation of α -Al grains^[22,23]. However, TiB_2 tends to aggregate into clusters and settle into the Al melt^[24], while TiC is destabilized in a portion of the Al melt to generate Al_4C_3 ^[25]. The Al-V-B master alloy containing VB_2 and VAI_3 particles can significantly refine the aluminum alloy, and VB_2 particles are the effective nucleation cores for the refinement of Al-7wt.% Si alloy^[26]. Furthermore, its refining effect is significantly better than the traditional Al-Ti-B and Al-Ti-C master alloys^[27]. Research has shown that V can refine the spacing between secondary dendrite arms^[28]. In recent years, scholars have refined Al-Si and Mg-Al alloys by adding Al-V-B master alloy. As stated by Ruan et al.^[29], the refinement effect of Al-V-B master alloys was more

*Guang-zong Zhang

Ph. D. His research interests mainly focus on the design and development of aluminum alloy grain refiners, high-valued utilization of aluminum based solid wastes, and the WAAM of aluminum and magnesium alloys. He has won the First Prize in Science and Technology of the Nonferrous Metals Industry Association in 2022.

E-mail: gzzhang@djtu.edu.cn

Received: 2023-10-18; Revised: 2023-12-09; Accepted: 2024-07-29

excellent than the Al-Ti-B master alloy, and the Al-(Ti+V)-B significantly reduced the grain size of Al-7Si from 854.6 to 136.93 μm . Allen et al. [30] found that, the combination of V and Al-Ti-B promoted heterogeneous nucleation in commercial ingots. Zhang et al. [31] prepared Al-3V-1.28B alloy containing VAI_3 and VB_2 particles, which reduced the size of Al-7Si alloy to 280 μm . Al-V-B and Al-5V-B refiners prepared by Li et al. [32] significantly reduced the grain size of Al-10Si alloy from 1,736 μm to 184–245 μm . Based on above literatures, Al-V-B master alloys can provide effective nucleation particles such as VB_2 and VB. However, master alloys that can provide both TiB_2 and VB_2 are rarely studied. Continuous rheological extrusion (CRE) technology, as an advanced material processing technique, is highly necessary for the production of grain refiners [24]. By integrating the advantages of plastic working and semi-solid forming, CRE technology enables continuous production, significantly simplifying the process and reducing costs. The high shear deformation and rapid cooling inherent in this technology effectively refine grains and prevent compositional segregation, thereby enhancing the performance and stability of grain refiners.

In this study, an Al-Ti-V-B master alloy containing particles of VB_2 , VB, and TiB_2 was designed, and its refinement effect of Al-Ti-V-B on A356 alloy was discussed. The effects of master alloy addition and the holding time on the microstructure and mechanical properties of A356 alloy were analyzed. The optimal parameters for utilizing the Al-Ti-V-B master alloy as a refiner were obtained. Additionally, the mechanism responsible for the generation of the refined phase was explored.

2 Experiment

2.1 Design and preparation of CRE Al-Ti-V-B alloy

Firstly, the Equilib module of FactSage 8.3 software (FTlite database) was employed to determine the generation of the physical phases in the equilibrium state of CRE Al-Ti-V-B, as illustrated in Fig. 1(a). Secondly, the standard Gibbs free energy (ΔG^0) for possible reactions in the CRE Al-Ti-V-B system was calculated using the Reaction module and is demonstrated in Fig. 1(b). The lower standard Gibbs free energy of the TiB_2 and TiAl_3 phases compared to the VB, VB_2 and VAI_3 phases suggests that Ti-containing phases such as TiB_2 and TiAl_3 are more stable than V-containing phases such as VB, VB_2 , and VAI_3 . It is also noteworthy that VB compounds are not stable in comparison to VB_2 , and will form VB_2 with B.

2.2 Experimental procedure

The experiment includes the preparation of grain refiner and refining experiment of A356 alloy. For the preparation of grain refiner, high-purity aluminum (99.95%), K_2TiF_6 , KBF_4 , Al-10V, and cryolite were weighed according to their mass percentages. As shown in Fig. 2, the high-purity aluminum was placed in the clay crucible and heated to 750 $^\circ\text{C}$. K_2TiF_6 and KBF_4 were added into the melt, and stirring was maintained for 1 h using a titanium alloy bar. Then, the temperature was raised to 1,200 $^\circ\text{C}$ and a mixture of Al-10V and KBF_4 was added before cryolite. After the reaction was completed, the melt

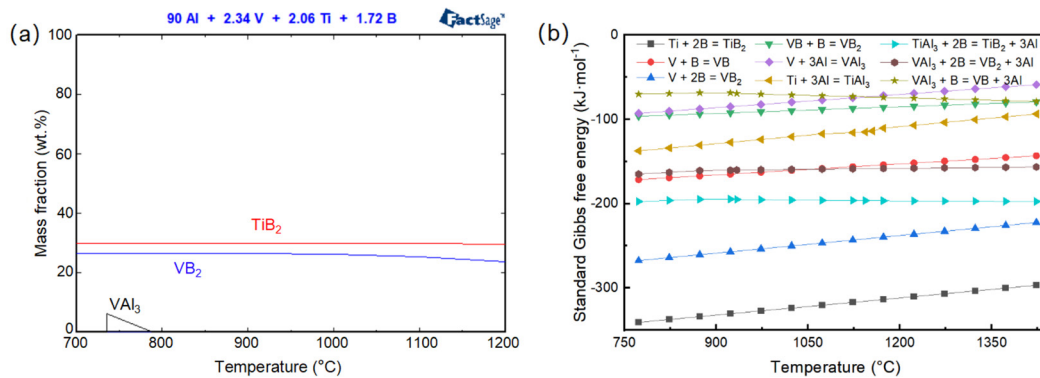


Fig. 1: Thermodynamic calculation of CRE Al-Ti-V-B intermediate alloy: (a) phase formation in equilibrium state; (b) standard Gibbs free energy of reaction ($\text{kJ}\cdot\text{mol}^{-1}$)

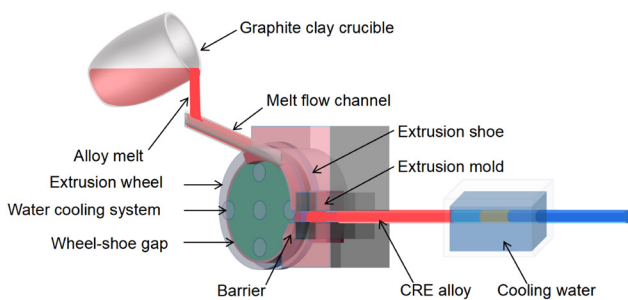


Fig. 2: Schematic diagram of preparation of CRE Al-Ti-V-B master alloy

was cooled to 780 $^\circ\text{C}$ and the slag was removed. The melt was poured into a continuous rheological extruder, and the speed was 7 $\text{rad}\cdot\text{min}^{-1}$. CRE Al-Ti-V-B master alloy with a diameter of 8.5 mm was obtained.

For the refining experiment of A356 alloy, as shown in Fig. 3, the dried A356 alloy was put into the graphite crucible and then put into a resistance furnace to be heated to 750 $^\circ\text{C}$. After melting, different amounts of CRE Al-Ti-V-B master alloys (0wt.%, 0.2wt.%, 0.3wt.%, 0.4wt.%, and 0.6wt.%) were added into A356 alloy. To prevent the aggregation and sedimentation of particles such as VB_2 and TiB_2 , the melt was stirred every 3 min for 2 min and then held for 5, 20, 40, 60, and

80 min, respectively. Then, the melt was poured into the mold preheated to 180 °C and cooled to room temperature. The dimensions of the molds, samples, and sampling locations are shown in Figs. 3(b, c).

Chemical compositions of master alloys tested by inductively coupled plasma-optical emission spectrometer (ICP-OES, PerkinElmer Avio500) are listed in Table 1. The samples were polished and mechanically polished. The phases in the samples were detected using X-ray diffractometer (XRD, Panalytical Empyrean) with a data acquisition range of 20°–90° at a scanning speed of 10°·min⁻¹. The grain size of

the alloy was measured and evaluated using Image Pro Plus software on images observed by an optical microscope (OM, Leica DMI8 A). Microstructure analysis was performed using a field emission scanning electron microscope (SEM, Zeiss Ultra Plus). The sub-microscopic structure of samples was observed using a transmission electron microscope (TEM, JEM-2100F).

3 Results and discussion

3.1 Microstructure of CRE Al-Ti-V-B master alloy

Figure 4 shows the XRD patterns of CRE Al-Ti-V-B master alloy. The second phase includes VB and VAl₃ phases in addition to VB₂ and TiB₂. This differs from the calculated results in Fig. 1(a). The CRE Al-Ti-V-B system does not reach full physical phase equilibrium mainly due to the low content of VB and VAl₃ in the melt and the short reaction time. The presence of these phases is crucial for achieving equilibrium, but their limited availability and insufficient time for reaction hinder the system from reaching a fully equilibrated state.

Figures 5(a–d) illustrate the microstructure of the CRE Al-Ti-V-B intermediate alloy. The alloy is primarily

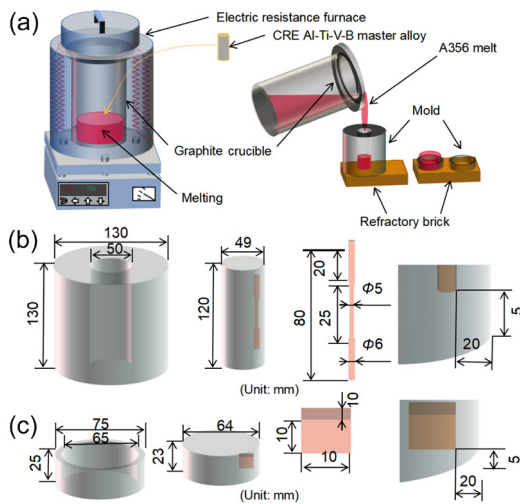


Fig. 3: Schematic diagram of A356 refinement (a), and sizes of mold and samples as well as sampling locations (b and c)

Table 1: Chemical compositions of CRE Al-Ti-V-B master alloy (wt.%)

Grain refiner	Ti	V	B	Al
CRE Al-Ti-V-B	2.06	2.34	1.72	Bal.

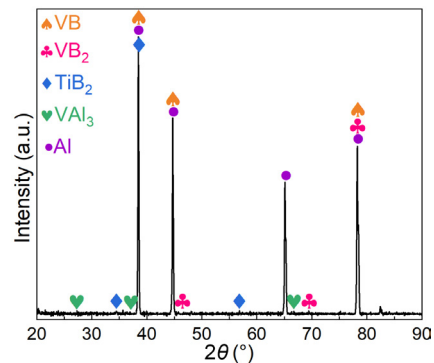


Fig. 4: XRD pattern of CRE Al-Ti-V-B master alloy

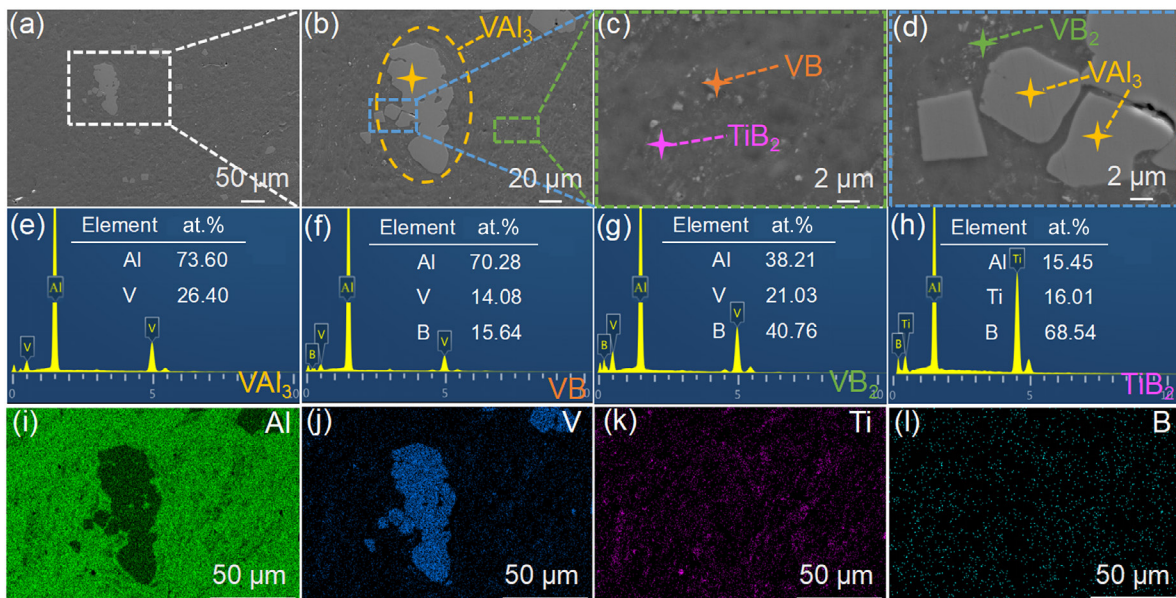


Fig. 5: SEM images and EDS results of CRE Al-Ti-V-B master alloy: (a–d) SEM images of Al-Ti-V-B master alloy; (e–h) EDS results for points VAl₃, VB, VB₂, and TiB₂; (i–l) EDS mapping of Al-Ti-V-B master alloy

composed of fine particulate matter and a minor quantity of lumps. The EDS analysis results in Fig. 5(e) indicate that the lumps are predominantly composed of Al, V and have an atomic percentage of approximately 3:1. Therefore, it can be postulated that the lumps are VAI_3 . Figures 5(f-h) indicate that the particulate matter is primarily B-containing compounds. In conjunction with the XRD patterns in Fig. 4, it can be postulated that the particulates are a combination of VB, VB_2 , and TiB_2 . Furthermore, the EDS mapping results in Figs. 5(i-l) demonstrate that the V element is concentrated in the VAI_3 phase, while the Ti element is concentrated in the fine particulate matter. Nevertheless, no $TiAl_3$ compounds are identified in the CRE Al-Ti-V-B alloy.

Figures 6(a) and (b) show the TEM images of the CRE Al-Ti-V-B master alloy. The HRTEM image is subjected to FFT transformation, as shown in Fig. 6(b), and the phase is determined as VB $[1, \bar{1}, \bar{2}]$. The selected area electron diffraction (SAED) patterns of TiB_2 in Figs. 6(a) and (c) show the enrichment of TiB_2 $[2, 1, 0]$ around the VB $[1, \bar{1}, \bar{2}]$ phase, which is consistent with the phenomena observed in Fig. 5. The HRTEM was performed, as shown in Figs. 6(h) and (j), and the crystal plane spacing d in the (110) direction is 0.284 nm, keeping consistent with the (110) direction of 0.289 nm in Ref. [33]. According to the EDS mapping in Figs. 6(d-g) and (i), Ti and B elements are distributed around the block VB phase. Moreover, the presence of fine nanophase containing both Ti and Al elements is $TiAl_3$ phase.

3.2 Refinement of A356 alloy by CRE Al-Ti-V-B

3.2.1 Effect of CRE Al-Ti-V-B addition

Figures 7(a-e) show the macrostructure and microstructure images of A356 alloy after introducing 0wt.%, 0.2wt.%, 0.3wt.%, 0.4wt.%, 0.6wt.% CRE Al-Ti-V-B and holding for 20 min. It might be worth noting that there is a density difference between the TiB_2 grain refinement particles ($\sim 4.5 \text{ g}\cdot\text{cm}^{-3}$ [34]) and the A356 melt ($2.6\text{--}2.7 \text{ g}\cdot\text{cm}^{-3}$ [35]), which can potentially lead to the particles sinking and making it challenging to maintain a uniform distribution of the grains. It may be helpful to consider that refinement particles such as TiB_2 have a greater tendency for heterogeneous nucleation, which can also contribute to the sinking of particles. When the content of CRE Al-Ti-V-B alloy is lower than 0.3wt.%, the grain refinement is proportional to the addition amount. Due to the aggregation of VB_2 and TiB_2 phases [36], when the CRE Al-Ti-V-B alloy addition exceeds 0.3wt.%, the number of effective refining phases in the melt decreases. Figure 7(f) shows the effect of CRE Al-Ti-V-B addition on the average grain size of the refined A356 alloy. As the addition of CRE Al-Ti-V-B alloy increases from 0 to 0.6wt.%, the average grain size of A356 alloy firstly decreases and then increases, and reaches a minimum value of $151.8\pm 9.11 \mu\text{m}$ at the addition of 0.3wt.%.

3.2.2 Effect of holding time

The effect of holding time on the refinement of A356 alloy was investigated (refiner content 0.3wt.%). Figures 8(a-e) show

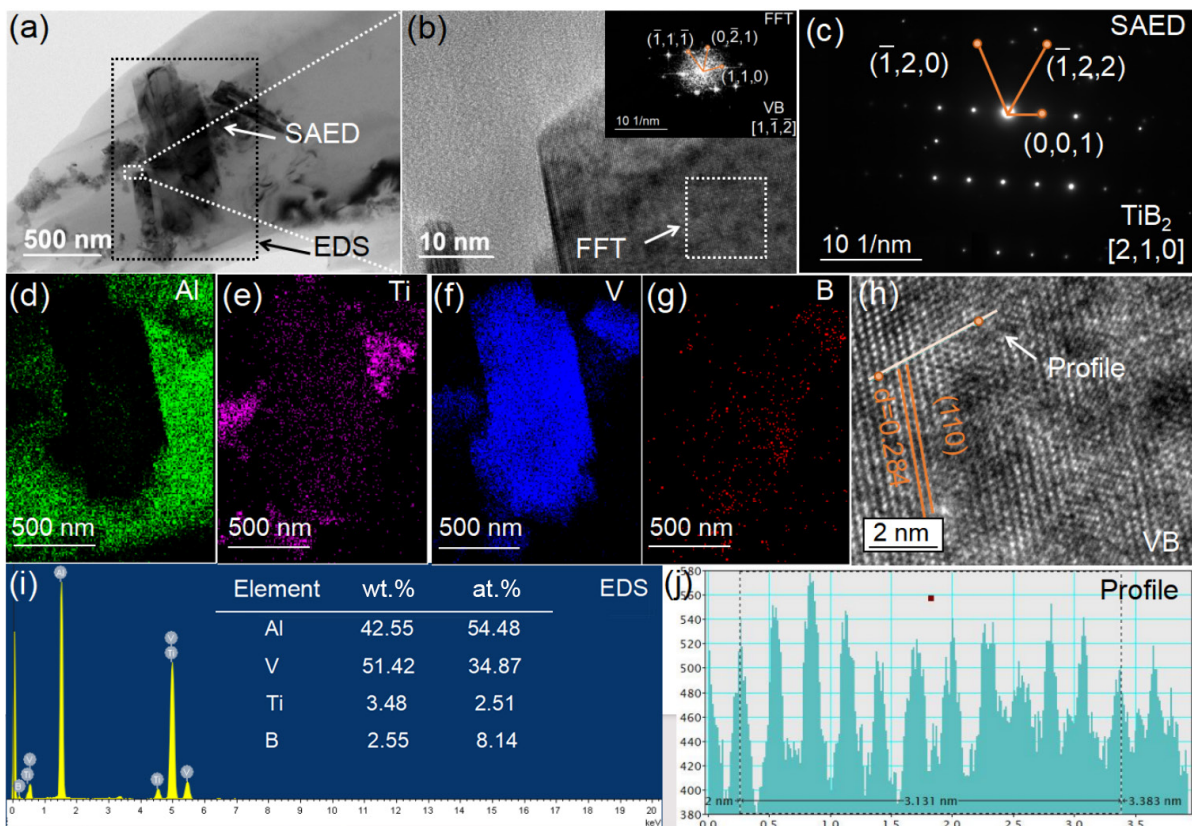


Fig. 6: TEM images and EDS results of CRE Al-Ti-V-B master alloy: (a) TEM photographs; (b) HRTEM photographs and FFT photographs of VB phase; (c) SAED photographs of TiB_2 phase; (d-g) and (i) EDS result; (h) HRTEM image of VB phase; (j) (110) orientation of profile of HRTEM image

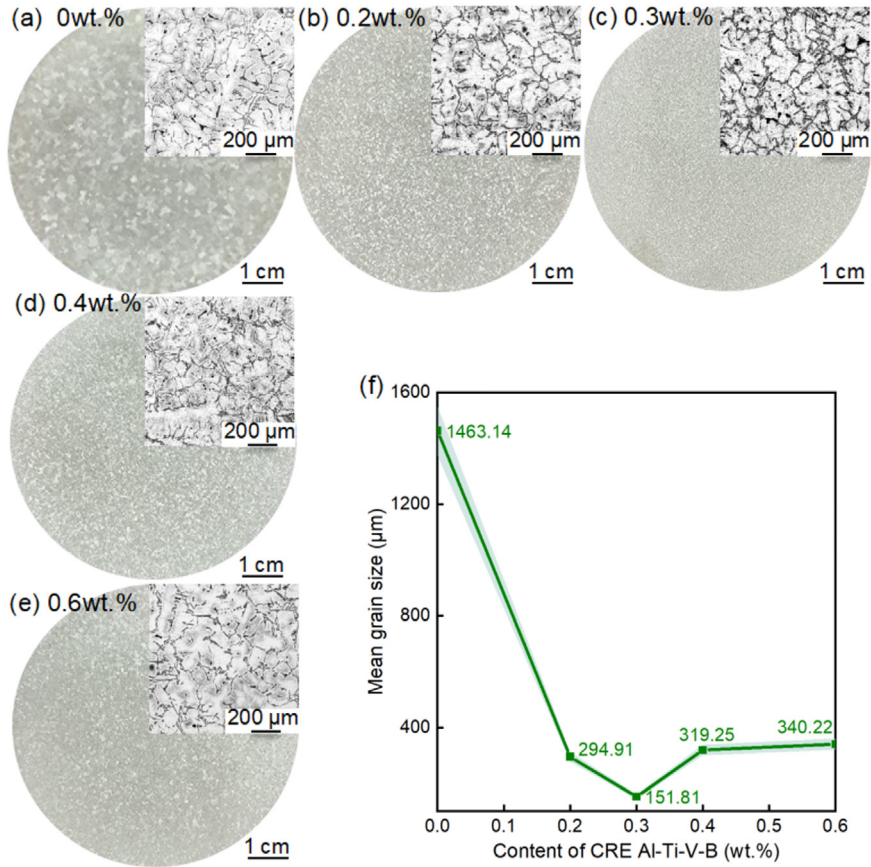


Fig. 7: Effect of CRE Al-Ti-V-B addition on the refinement of A356 alloy: (a) 0wt.%; (b) 0.2wt.%; (c) 0.3wt.%; (d) 0.4wt.%; (e) 0.6wt.%; (f) average grain size

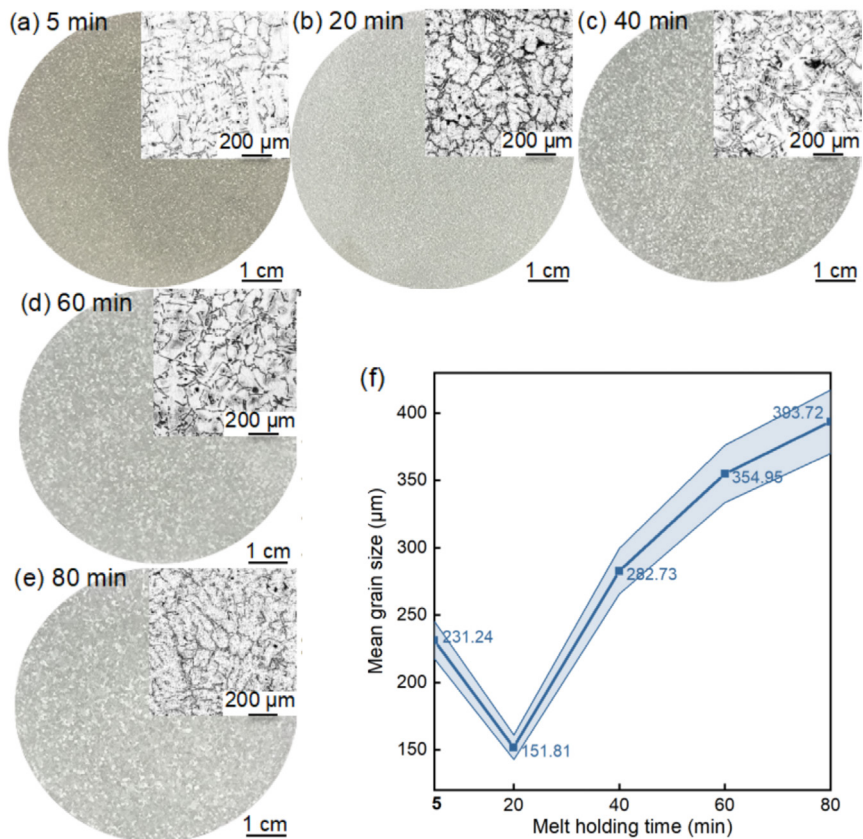


Fig. 8: Effect of holding time on the refinement of A356 alloy: (a) 5 min; (b) 20 min; (c) 40 min; (d) 60 min; (e) 80 min; (f) average grain size

the macro- and microscopic images of A356 ingots at holding times of 5, 20, 40, 60, and 80 min, respectively. Figure 8(f) shows the effect of holding time on the average grain size of the refined A356 alloy.

As shown in Figs. 8(a-e), the average grain size evolves non-monotonically as the holding time increases from 5 to 80 min, and reaches a minimum value of $151.8 \pm 9.11 \mu\text{m}$ at 20 min. Thus, under the optimum refiner addition amount of 0.3wt.% and the holding time of 20 min, the average grain size of the as-cast A356 alloy is $151.8 \pm 9.11 \mu\text{m}$. Aggregation of nucleated particles may lead to an increase of local supercooling [37-39]. The degree of subcooling affects the phase transition process. Components exceeding the critical content are confined in a nonequilibrium state, which leads to grain formation. Whereas, when the holding time is longer than 20 min, the aggregation of nucleating particles such as VB_2 and TiB_2 leads to the reduction of the number of effective nucleation in the melt, and the refinement is weakened [40, 41].

The introduction of the V element creates conditions for the formation of the second phases of VB_2 and VB. It has been reported that, VB_2 particles are a component of the $\text{VB}_2\text{-AlB}_2$ core-shell structure and serve as nucleation particles for refining Al-Si alloys [42]. VB particles enhance the mechanical properties of Al-12.6wt.% Si based composites [43]. McCartney [44] presented a simplified expression for the nucleation rate of the VB and VB_2 precipitates formed from a liquid alloy:

$$I = CN_v^p \exp\left[\frac{-16\pi\sigma_a f(\theta)}{3k_B\Delta S^2\Delta T^2}\right] \quad (1)$$

where C is the coefficient relevant to atomic diffusion, N_v^p is the number of embryos per unit volume of the melt, σ_a is the liquid-solid interfacial tension, $f(\theta)$ is the wetting angle factor, k_B is the Boltzmann constant, ΔS is the nucleation entropy, and ΔT is the degree of nucleation undercooling.

Due to the introduction of CRE Al-Ti-V-B master alloy, the degree of supercooling increases, facilitating the increasing nucleation rate of VB_2 and VB and promoting the grain refinement of A356 aluminum alloy [44].

3.3 Mechanical properties of refined A356 alloys

Figure 9 shows the mechanical properties of the refined A356 alloy at different addition amounts and holding times. In Figs. 9(a) and (b), the mechanical properties of A356 alloy are the highest when the CRE Al-Ti-V-B addition is 0.3wt.% upon the holding time of 20 min. The tensile strength and elongation are 196.11 MPa and 5.75%, respectively. Also, as shown in Figs. 9(c) and (d), the tensile strength and elongation change non-monotonically with the holding time, and both obtain peak values at the holding time of 20 min and the CRE Al-Ti-V-B addition of 0.3wt.%. As mentioned above, holding time has an effect on the aggregation behavior of nucleation particles such as VB, VB_2 , and TiB_2 . When the holding time is short, the distribution of the nucleation particles is uneven. As the time prolongs, the nucleation particles disperse more homogeneously, which leads to a more excellent refinement effect, tensile strength and elongation [45]. However, an excessive longer holding time causes the nucleation particles aggregate into clusters [46], resulting in the worse refinement effect, and a decrease in mechanical properties of the alloys.

Figure 10 shows the effect of CRE Al-Ti-V-B refiner addition (0.3wt.% and 20 min) and T6 heat treatment on the mechanical properties of the refined A356 alloy. It can be found that, T6 heat treatment increases the tensile strength and decreases the elongation of the original and refined A356 alloys. The combination of the CRE Al-Ti-V-B refiner and T6 heat treatment results in a significant enhancement in the tensile strength of the refined A356 alloy, which should be attributed

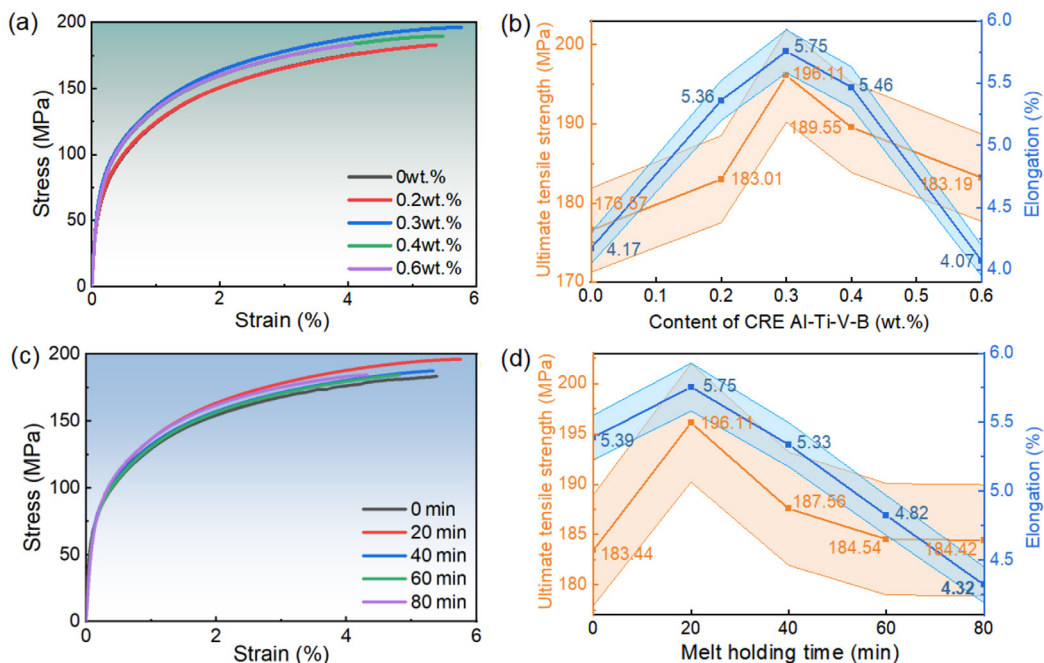


Fig. 9: Mechanical properties of refined A356 alloys at different addition amounts and holding times; (a, c) stress-strain curves; (b, d) tensile strength and elongation values; (a, b) holding time is 20 min; (c, d) CRE Al-Ti-V-B addition amount is 0.3wt.%

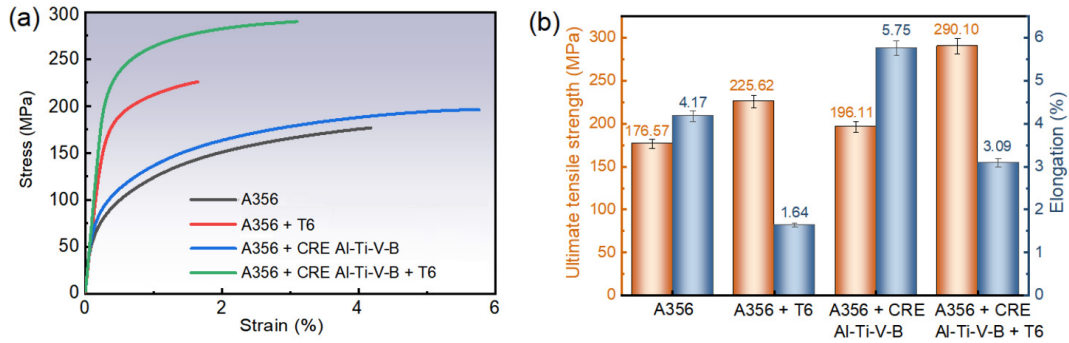


Fig. 10: Effect of CRE Al-Ti-V-B refiner addition and T6 heat treatment on the mechanical properties of refined A356 alloy: (a) stress-strain curves; (b) tensile strength and elongation

to the spheroidization of Si phase and the re-solubilization and precipitation of Mg_2Si [47, 48]. The strength increases from 196.11 MPa to 290.10 MPa, representing a 64.29% improvement over the original A356 alloy. Furthermore, due to the inverse relationship between tensile strength and elongation, the elongation decreases to 3.09% after T6 treatment.

3.4 Fracture morphology of A356 alloys

Figure 11 shows the fracture morphology of the A356 alloy under different treatments. The Al-Ti-V-B refiner was added at 0.3wt.% and held for 20 min. The occurrence of cleavage surface indicates the brittle fracture [49]. As shown in Figs. 11(a) and (b), T6 heat treatment has changed the fracture morphology upon the action on fracture edges [50-52], i.e., the cleavage surface is more obvious and the dimples become smaller and shallower. Compared Fig. 11(a) with Fig. 11(c), the addition of CRE Al-Ti-V-B alloy results in an increase

in the number of apparent tearing edges and an increase in the fraction of disintegrated surfaces. This phenomenon also suggests that the addition of CRE Al-Ti-V-B alloy improves the plasticity. Figure 11(d) shows the fracture morphology of the refined A356 alloy after T6 heat treatment, the higher fraction of cleavage surface indicates the lower plasticity.

Considering the higher tensile strength, the longitudinal fracture morphology of the refined A356 alloy under the coupling effect of CRE Al-Ti-V-B alloy and T6 heat treatment is analyzed and shown in Fig. 12. Combined with Figs. 12(a) and (b), under the stress action, stress concentration occurs within the grains and at grain boundaries. Further increasing the stress induces the separation of the alloy matrix, and causes the morphology characterization of composite pattern of along-crystal and through-crystal fracture [53, 54]. The effect of grain refinement on fracture should be explained as that, finer grains lead to crack path deflection, which increases energy

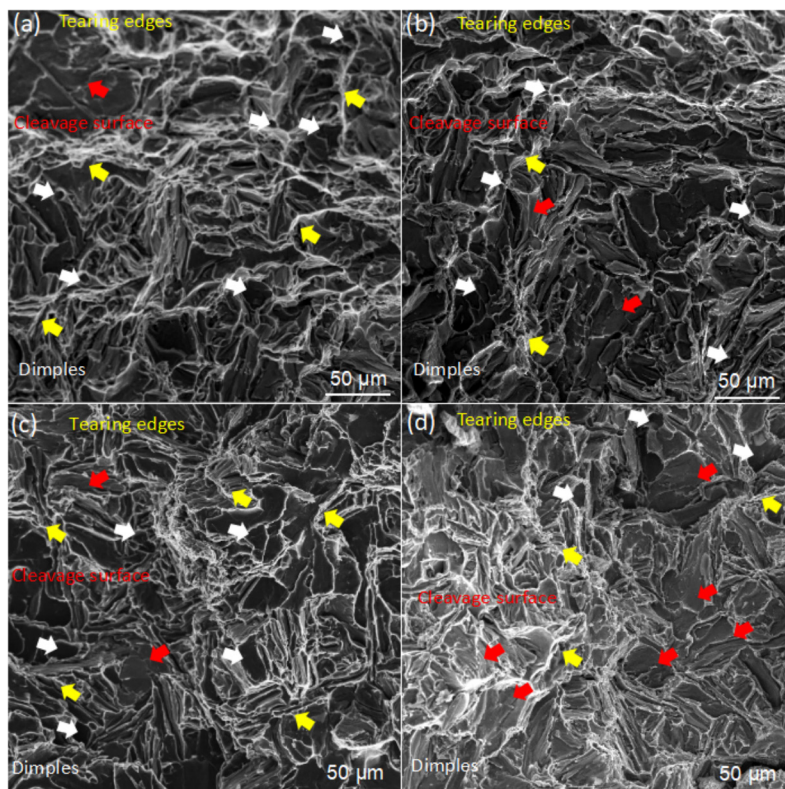


Fig. 11: Fracture morphology of A356 alloys: (a) original A356 alloy; (b) A356 alloy after T6 heat treatment; (c) refined A356 alloy; (d) refined A356 alloy after T6 heat treatment

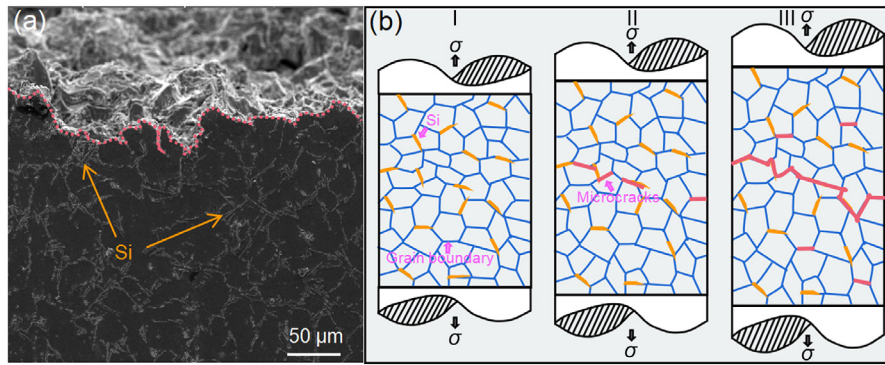


Fig. 12: Longitudinal fracture morphology of A356 alloy under the coupling effect of CRE Al-Ti-V-B alloy and T6 heat treatment: (a) refined A356 alloy after T6 heat treatment; (b) fracture mechanism

dissipation and reduces the tendency of brittle fracture. Also, finer grains improve the plasticity, which helps to produce localized plastic deformation in the stress concentration region, absorbing and dispersing the stress and reducing the probability of fracture along-crystal. Thus, under increasing stress, the fracture morphology of the alloy is characterized by the presence of small amount of along-crystal fracture.

4 Conclusions

This work focuses on the optimum refinement of as cast A356 alloy by continuous rheological extrusion (CRE) Al-Ti-V-B master alloy. Following conclusions are drawn:

(1) The optimum parameters are determined as CRE Al-Ti-V-B addition of 0.3wt.% and holding time of 20 min, and the grain size of the refined A356 alloy is $151.8 \pm 9.11 \mu\text{m}$, accordingly, 89.62% lower than that of original A356 alloy.

(2) Under the coupling effect of CRE Al-Ti-V-B refiner and T6 heat treatment, the tensile strength of refined A356 alloy increases to 290.1 MPa, 64.29% higher than that of original A356 alloy. Meanwhile, the elongation reaches 3.09%.

(3) The fracture morphology of the A356 alloy under the coupling effect of the CRE Al-Ti-V-B refiner and T6 heat treatment is characterized by a predominance of along-crystal fracture with a small amount of through-crystal fracture. This morphology is attributed to the refined grains, which promote crack path deflection and localized plastic deformation, enhancing energy dissipation and reducing the tendency for brittle fracture.

Acknowledgments

This work was supported by the National Key Research and Development Program of China (Grant No. 2022YFB3706801), the National Natural Science Foundation of China (Grant Nos. U2341253, 52371019, U2241232), the Dalian High-level Talents Innovation Support Program (Grant No. 2021RD06), the Applied Basic Research Program of Liaoning Province (Grant No. 2022JH2/101300003), and the Natural Science Foundation of Liaoning Province (Grant Nos. 2022-BS-262, JYTMS20230031).

Conflict of interest

The authors declare that they have no known competing financial interests or personal relationships that could have appeared to influence the work reported in this paper.

References

- [1] Liu W N, Zhang W, Wang P Y, et al. Effect of slow shot speed on externally solidified crystal, porosity and tensile property in a newly developed high-pressure die-cast Al-Si alloy. *China Foundry*, 2024, 21(1): 11–19.
- [2] Shahrooz N, Reza G. Grain refining of conventional and semi-solid A356 Al-Si alloy. *Journal of Materials Processing Technology*, 2006, 174(1–3): 371–383.
- [3] Fan Z Y, Gao F. Grain initiation and grain refinement: An overview. *Metals*, 2022, 12(10): 1728.
- [4] Wang F, Chiu Y L, Eskin D, et al. A grain refinement mechanism of cast commercial purity aluminium by vanadium. *Materials Characterization*, 2021, 181: 111468.
- [5] Vicario I, Angeline P, Lagos M A, et al. Effect of material and process atmosphere in the preparation of Al-Ti-B grain refiner by SHS. *Metals*, 2015, 5(3): 1387–1396.
- [6] Li D X, Yan X R, Fan Y, et al. An anti Si/Zr-poisoning strategy of Al grain refinement by the evolving effect of doped complex. *Acta Materialia*, 2023, 249: 118812.
- [7] Luo Q, Li X R, Li Q, et al. Achieving grain refinement of α -Al and Si modification simultaneously by La-B-Sr addition in Al-10Si alloys. *Journal of Materials Science & Technology*, 2023, 135: 97–110.
- [8] Zhao Z Y, Li D X, Zhang D Q, et al. Enhancement of the strength-ductility synergy of Al-Si-Mg alloys via C-doped TiB_2 particles. *Materials Letters*, 2022, 328: 133094.
- [9] Srivastava N, Chaudhari G P. Grain refinement in ultrasonicated binary aluminum alloys. *Journal of Crystal Growth*, 2020, 125415.
- [10] Kundu A, Biswas P, Sahu M, et al. Effect of electromagnetic flow direction on grain refinement of Al 2024 alloy. *JOM*, 2023, 75(8): 2799–2817.
- [11] Ma K, Zhao Y H, Xu X L, et al. Grain refinement mechanism at high undercooling of Ni80Cu20 alloy. *Materials Research Express*, 2019, 6(4): 046522.
- [12] Simões F, Leal R M, Rodrigues D M, et al. Grain size refinement of copper DHP by solid state processing. *Microscopy and Microanalysis*, 2013, 19(S4): 127–128.
- [13] Wang Y, Wang J N, Xia Q F, et al. Microstructure refinement of a TiAl alloy by heat treatment. *Materials Science and Engineering: A*, 2000, 293(1): 102–106.

- [14] Kimberly S L, Ralf B B, Andreas B. Nonequilibrium grain size distribution with generalized growth and nucleation rates. *Journal of Materials Research*, 2013, 28: 1407–1412.
- [15] Jiang H X, Sun Q, Zhang L L, et al. Al-Ti-C master alloy with nano-sized TiC particles dispersed in the matrix prepared by using carbon nanotubes as C source. *Journal of Alloys and Compounds*, 2018, 748: 774–782.
- [16] Gan G S, Yang B, Zhang B, et al. Refining mechanism of 7075 Al alloy by in-situ TiB₂ particles. *Materials*, 2017, 10(2): 132.
- [17] Backerud L, Shao Y D. Grain refining mechanisms in aluminium as a result of additions of titanium and boron. I. *Aluminium*, 1991, 67(7–8): 780–785.
- [18] Wang F, Liu Z L, Qiu D, et al. Revisiting the role of peritectics in grain refinement of Al alloys. *Acta Materialia*, 2013, 61(1): 360–370.
- [19] Mohanty P S, Gruzleski J E. Mechanism of grain refinement in aluminium. *Acta Metall. et Mater.*, 1995, 43(5): 2001–2012.
- [20] Wang F, Qiu D, Liu Z L, et al. The grain refinement mechanism of cast aluminium by zirconium. *Acta Materialia*, 2013, 61(15): 5636–5645.
- [21] Dobeš F, Dymáček P, Friák M, et al. The influence of niobium additions on creep resistance of Fe-27 at.% Al alloys. *Metals*, 2019, 9(7): 739.
- [22] Cibula A. The grain refinement of aluminium alloy castings by additions of titanium and boron. *J. Inst. Metals*, 1951, 80: 1–16.
- [23] Zarrinfar N, Shipway P, Saidi A, et al. Carbide stoichiometry in TiC_x and Cu-TiC_x produced by self-propagating high-temperature synthesis. *Scripta Materialia*, 2002, 46: 121–126.
- [24] Guan R G, Tie D. A review on grain refinement of aluminum alloys: Progresses, challenges and prospects. *Acta Metallurgica Sinica (English Letters)*, 2017, 30(5): 409–432.
- [25] Birol Y. Grain refining efficiency of Al-Ti-C alloys. *Journal of Alloys and Compounds*, 2006, 422(1): 128–131.
- [26] Zhang Y H, Ye C Y, Shen Y P, et al. Grain refinement of hypoeutectic Al-7wt.%Si alloy induced by an Al-V-B master alloy. *Journal of Alloys and Compounds*, 2019, 812: 152022.
- [27] Fan W X, Bai Y, Zuo G L, et al. Enhanced grain refinement and mechanical properties of AZ91 alloy by a novel Al-5.1V-2.3B refiner containing VB₂ and VB particles. *Materials & Design*, 2023, 225: 111474.
- [28] Liu L, Zhao J, Zhan H, et al. High-temperature in-situ synthesis and formation mechanism of VB₂ substrates in Al-V-B grain refiner. *Materials Today Communications*, 2023, 34: 105281.
- [29] Ruan Q L, Meng C C, Xie Z S, et al. Effect of (Ti+V)B₂ on the grain structure of Al-7Si alloy. *Transactions of the Indian Institute of Metals*, 2023, 76: 2765–2771.
- [30] Allen C M, O'reilly K A Q, Evans P V, et al. The effect of vanadium and grain refiner additions on the nucleation of secondary phases in 1xxx Al alloys. *Acta Materialia*, 1999, 47(17): 4387–4403.
- [31] Zhang Y H, Ye C Y, Shen Y P, et al. Grain refinement of hypoeutectic Al-7wt.%Si alloy induced by an Al-V-B master alloy. *Journal of Alloys and Compounds*, 2020, 812: 152022.
- [32] Zhao C X, Li Y, Xu J, et al. Enhanced grain refinement of Al-Si alloys by novel Al-V-B refiners. *Journal of Materials Science & Technology*, 2021, 94: 104–112.
- [33] Parthe E, Schob O. New compounds. Vanadium monoboride. *Journal of the American Chemical Society*, 1952, 74(11): 2942.
- [34] Vinod Kumar G S, Murty B S, Chakraborty M. Settling behaviour of TiAl₃, TiB₂, TiC and AlB₂ particles in liquid Al during grain refinement. *International Journal of Cast Metals Research*, 2010, 23: 193–204.
- [35] Wu X Y, Zhang H R, Ma Z, et al. Effect of holding pressure on microstructure and mechanical properties of A356 aluminum alloy. *Journal of Materials Engineering and Performance*, 2018, 27: 483–491.
- [36] Schaffer P L, Dahle A K. Settling behaviour of different grain refiners in aluminium. *Materials Science and Engineering: A*, 2005, 413–414: 373–378.
- [37] Chalamet L, Rodney D, Shibuta Y, et al. Coarse-grained molecular dynamic model for metallic materials. *Computational Materials Science*, 2023, 228: 112306.
- [38] Yang Y, Li S R, Liang Y X, et al. Effect of temperature on wetting kinetics in Al/SiC system: A molecular dynamic investigation. *Composite Interfaces*, 2020, 27(6): 587–600.
- [39] Harish S M, Patra P K. Temperature and its control in molecular dynamics simulations. *Molecular Simulation*, 2021, 47(9): 701–729.
- [40] Gábor G, Levente B, Marcin S, et al. Grain refiner settling and its effect on the melt quality of aluminum casting alloys. *Materials*, 2022, 15: 7679.
- [41] Schaffer P L, Dahle A K. Settling behaviour of different grain refiners in aluminium. *Materials Science and Engineering: A*, 2005, 413-414: 373–378.
- [42] Zhao C X, Li Y, Xun J, et al. Enhanced grain refinement of Al-Si alloys by novel Al-V-B refiners. *Journal of Materials Science & Technology*, 2020, 94: 104–112.
- [43] Emre T, Duygu A, Siddika M, et al. Microstructural characterizations and mechanical properties of NbB₂ and VB particulate-reinforced eutectic Al-12.6 wt.% Si composites via powder metallurgy method. *Advanced Powder Technology*, 2018, 29(9): 2070–2081.
- [44] McCartney D G. Grain refining of aluminium and its alloys using inoculants. *International Materials Reviews*, 1989, 34: 247–260.
- [45] Li P, Wang L S, Wang B, et al. Diffusion and mechanical properties of Ti₂AlNb and TiAl₁₅ interface: From experiments to molecular dynamics. *Vacuum*, 2022, 195: 110637.
- [46] Christian L, Christoph D. Nucleation and structural growth of cluster crystals. *The Journal of Chemical Physics*, 2016, 145: 074504.
- [47] Liu G Q, Wang Q D, Liu T, et al. Effect of T6 heat treatment on microstructure and mechanical property of 6101/A356 bimetal fabricated by squeeze casting. *Materials Science and Engineering: A*, 2017, 696(1): 208–215.
- [48] Ridvan G, Serhat A, Alptekin K, et al. Influence of T6 heat treatment on A356 and A380 aluminium alloys manufactured by thixoforging combined with low superheat casting. *Transactions of Nonferrous Metals Society of China*, 2018, 28(3): 385–392.
- [49] Kumar S, Tewari S P. Evaluation of microstructure of A356 aluminum alloy casting prepared under vibratory conditions during the solidification. *Sādhanā*, 2016, 41: 1203–1208.
- [50] Liu Y L, Wu C J, Tu H, et al. Microstructure and mechanical properties of Al-10Si alloy modified with Al-5Ti. *China Foundry*, 2018, 15(6): 405–410.
- [51] Uludağ M. Influence of Al-B grain refiner on porosity formation of directionally solidified Al-Si alloys. *China Foundry*, 2020, 17(5): 372–377.
- [52] Hu X P, Zhao Y, Wang Q, et al. Effect of pouring and cooling temperatures on microstructures and mechanical properties of as-cast and T6 treated A356 alloy. *China Foundry*, 2019, 16(6): 380–385.
- [53] Han S, Lezaack M B, Pyka G, et al. On the competition between intergranular and transgranular failure within 7xxx Al alloys with tailored microstructures. *Materials*, 2023, 16(10): 3770.
- [54] Xiao L, Yang G Y, Ma J Q, et al. Microstructure evolution and fracture behavior of Mg-9.5Gd-0.9Zn-0.5Zr alloy subjected to different heat treatments. *Materials Characterization*, 2020, 168: 110516.